Supporting Online Material for

Reassessment of the Potential Sea-Level Rise from a Collapse of the West Antarctic Ice Sheet

Jonathan L. Bamber,* Riccardo E. M. Riva, Bert L. A. Vermeersen, Anne M. LeBrocq

*To whom correspondence should be addressed. E-mail: j.bamber@bristol.ac.uk

Published 15 May 2009, *Science* **324**, 901 (2009)
DOI: 10.1126/science.1169335

This PDF file includes:

Supporting Online Material

1. Initial Considerations

In the early studies on WAIS instability it was suggested that a "warning sign of dangerous warming in the Antarctic" would be the break up of ice shelves in the Peninsula (S1). This has already taken place for parts of the Larsen ice shelf resulting in a marked increase in discharge rates of the inland, grounded ice (S2, 3). Most recently Wilkins Ice Shelf has begun to disintegrate and the Peninsula ice shelves are clearly vulnerable to recent, marked oceanic and atmospheric warming. The large Filchner Ronne and Ross ice shelves that buttress much of the West Antarctic Ice Sheet (WAIS) are colder and thicker than their Peninsula neighbours and there is no evidence to suggest that they are in danger of break-up. Nonetheless, there is evidence of retreat in West Antarctica that comes from recent satellite observations of elevation change and ice motion. These observations indicate that the Amundsen and Bellinghausen Sea sectors of the WAIS are losing on the order of 100 Gt a^{-1} of ice, most likely as a consequence of enhanced oceanic melting of buttressing ice shelves and the impact of this on the backstress felt by the inland grounded ice (S4). It has also been observed that the grounding line of Pine Island Glacier has retreated at a rate of 1.2 km a^{-1} between 1992 and 1996 (S5), in good agreement with a predicted value of 1.5 km a^{-1}, from a model of WAIS collapse (S6). The various satellite observations, however, cover a limited period of between ~15 and 30 years and it is, currently, unknown whether they represent a longer-term secular trend. They demonstrate, nonetheless, the sensitivity of inland ice dynamics to changes in ice shelf conditions and, in so doing, point to a mechanism for rapid mass loss from the WAIS (S7) and have re-ignited the debate about the possible instability of the WAIS (S8). No whole ice sheet models adequately incorporate the key processes that underpin the marine ice sheet instability (MISI) hypothesis. In particular, they do not include longitudinal stresses nor adequate treatment of grounding line retreat although theoretical advances have been made in both these areas (S9-11). As a consequence, whole ice sheet models cannot, currently, be used to test or simulate the MISI hypothesis. The potential contribution to SLR of a collapse of the WAIS is, however, an issue of great concern for risk assessment studies, as well as understanding past SLR. The generally accepted value appears to originate from a paper by Mercer in 1978 (S1). The value quoted is 5 m, and, itself, appears to be derived from a study published ten years earlier that was largely based on paleo-evidence of former sea level high stands (S12). Despite major advances in our knowledge of surface and bed topography of Antarctica, no quantitative, glaciologically-consistent reassessment appears to have been undertaken since then. Here, we take a conceptual approach to assess the likely contribution based on glaciological and topographic constraints and theory.

2. Calculation of the ROI and ice volumes

The extent of the WAIS susceptible to collapse has never been clearly or explicitly defined in previous studies. Here, we attempt to do this using a conceptual approach but relaxing, in particular, the negative bed slope condition discussed below to provide what we consider, therefore, to be an upper bound to the region susceptible to a collapse as a result of the MISI hypothesis (i.e. as opposed to other dynamic processes or surface mass loss). We also consider other cases, such as complete removal of all WAIS ice, grounded above or below sea level and the case where the negative bed slope condition is applied stringently. We do

not consider, however, the case of a partial collapse of the ice sheet that might be associated, for example, with wastage of the Amundsen Sea sector (S8). Neither do we consider areas of East Antarctica that are marine based (Fig. 1 and Fig. S1). These include the Wilkes subglacial trench, drained by Cook Glacier, and Ninnis, Mertz, Thompson and Totten Glaciers. Several of these outlets show signs of recent thinning (S13).

Three principal conditions were used to identify the region of interest (ROI). The first was bed elevation below sea level (BSL). The second was whether the bed slope was negative inland from the direction of ice motion (plus or minus 30º). In other words, whether bed elevations decreased up-glacier from the grounding line. These two conditions were used to define grid cells that were considered to satisfy the Marine Ice Sheet Instability (MISI) condition. The third condition was that the first two conditions must be satisfied close (within 20 ice thicknesses) to the grounding line. We note that parts of the Recovery, Bailey and Slessor Glacier catchments that feed into the Filchner ice shelf satisfy the first two conditions but not the third (Fig. S1). We also note that a thick, likely marine, sedimentary basin has been postulated beneath an inland section of Slessor glacier (S14) and that a deep basin, not resolved in the BEDMAP data set, lies beneath part of Recovery Glacier (S15, 16). Calculations were carried out on 5 km resolution grids of surface elevation and ice thickness initially for the whole of Antarctica (Fig. S1). The direction of ice motion was determined by assuming ice flows downhill over a length scale where the influence of longitudinal stresses can be ignored. To achieve this, the surface topography was smoothed using an exponential distance weighting with a length scale of 25 times the ice thickness (S17). Bed elevations were compared over a distance of 50 km within ±30º of the present-day smoothed flow direction, determined from the ice surface slope aspect. If the bed elevation was lower for the “upstream” grid cell, the point was considered to satisfy the MISI condition. The results were relatively insensitive to the scale lengths used. Fig. S1 shows the result of this calculation for the whole of the WAIS and those basins in the EAIS that drain into the Filchner Ronne and Ross ice shelves.

It is evident that the areas that satisfy the MISI condition, as defined above, are not continuous, which is not always physical. Rapid grounding line migration and drawdown will affect inland ice over length scales where longitudinal stresses are important. This length scale depends on the ice rheology and the slip ratio (ratio of velocity due to basal motion compared with velocity due to internal deformation) increasing with increasing slip ratio. We, therefore, merged adjacent contiguous areas where the MISI condition was satisfied. We did not allow grounding lines to exist below 1000 m BSL, which is similar to the maximum depth of contemporary grounding lines for the WAIS. Finally, we excluded areas that were not within 20 ice thicknesses of the grounding line and, at this stage, also limited the ROI to the WAIS and ice streams feeding the Filchner Ronne and Ross ice shelves. Thus, isolated inland “hollows” were excluded. This resulted in the mask shown in Fig. S2. We consider this to be a liberal estimate of the area of the WAIS that satisfies the MISI condition, excluding only the marginal areas close to ice grounded above sea level where bed elevations are greater than -1000 m and which do not have negative bed slopes (the dark grey areas in Fig S2). It is not meant to be a definitive estimate of the area susceptible to grounding line migration. An estimate of this is better suited to a numerical modeling study that incorporates longitudinal stresses and an appropriate representation of

grounding line behavior. As no such model exists, we use the mask shown in Fig S2 to give what we believe is an upper estimate for the ROI.

Three fairly contiguous “ice caps” remain in the ROI and the margins of these will respond to drawdown of surrounding ice. Rather than a vertical “cliff” at the edge of these ice caps we have assumed that they relax to a new equilibrium profile calculated using a modified version of a thermo-mechanical ice sheet model called GLIMMER (S18). The modified version of GLIMMER uses differing sliding relations for ice grounded above and below sea level, as a proxy for ‘hard bed’ sliding and ‘soft bed’ sliding respectively. Where the ice is grounded above sea level, the sliding relation is a linear function of the driving stress. Where the ice is grounded below sea level, a measure of the effective pressure is incorporated into the sliding relation, allowing the reconstruction of the typical concave ice surface profiles found in the WAIS. The sliding parameters for the two sliding relations were derived from calibration with the present day ice sheet surface. We imposed the condition that the new grounding lines must satisfy hydrostatic equilibrium and this provides the surface elevation boundary condition at the margins. Two simulations were undertaken: one to reproduce the present-day ice sheet and the second forcing the collapsed portions of the ROI to be ice free. The volume of ice drawdown was calculated as the difference between the two simulations, and is shown in Fig. S4. Interestingly, the estimate for the extant ice within the WAIS (53 cm) is similar to an earlier estimate (60 cm), which was obtained by fitting a Vialov-type parabolic profile to the extant regions (S19). Examples, of the original and new surface profiles for the Marie Byrd Land ice cap are shown in Fig. S5. A further 41 cm results, after ~10000 years, from the drawdown of ice around and inland from Recovery Glacier and Foundation Ice Stream (Fig S4) and we have added half of this total to the short-term (100-1000 year) SLR estimate (Table S1). This results in a total drawdown contribution of 74 cm. Finally, we assume that there will be a dynamic response of grounded outlet glaciers and ice streams to the loss of the buttressing effect of the ice shelves and this is discussed in section 2 below and Table S1. We consider our estimates of these two effects to be liberal, as the they are secondary, ice flow responses to the first-order instability hypothesis proposed for the rest of the WAIS and, importantly, we assume an instantaneous removal of “MISI” sectors in our drawdown and dynamic response calculation. In reality, the large volumes of ice that will need to be evacuated would become grounded in the Ross and Filchner Ronne embayments, slowing both the drawdown and dynamic response (S20).

A correction, although relatively small, is required to account for the depth and density of the firn layer. This is not a constant and was calculated here from the output of a regional climate model (S4, 21). The correction affects only the mass of ice above the geoid calculated and, subsequently, the mass of ice that contributes to eustatic SLR. It reduces the total mass entering the ocean (compared with the assumption of a mean ice density for the whole column above sea level of 918 kg m^{-3}) by 2%, or ~ 7 cm.

3. Uncertainties in estimating the volume and mass of the ROI

The mean surface elevation of the ROI is 1001 m asl. This is the mean thickness of ice that will contribute to SLR (after correcting for the density difference between sea water and ice for the inundated area of the ROI). Errors in the surface DEM scale linearly with this value.

Thus a 1 m bias introduces a 0.1% error in the volume estimate contributing to SLR. Similarly the mean firn depth correction, mentioned above, is 18.8 m, which is 2% of the mean thickness above sea level. Biases in the surface DEM have been assessed using independent *in-situ* data and are at a decimeter level (S4). Similarly for the geoid used. Errors in the bed topography primarily affect the estimate of the ROI. To assess this, we shifted the bed elevations by the quoted RMS error in thickness calculated for the WAIS from BEDMAP (±136 m) (S22) and recalculated the ROI and ice mass from the revised ROI. It should be noted that we have included more recent thickness data, compared to the BEDMAP compilation, for the largest basins in the WAIS, Pine Island and Thwaites and this will reduce the overall uncertainty for ~ 25% of the ROI. The uncertainty in bed elevation gives a range of +19 cm to –20 cm in terms of SLR equivalent.

There is no scientific argument or basis for suggesting that the sectors of the WAIS with a positive bed slope or grounded above sea level are inherently unstable and, indeed, almost all of the EAIS satisfy one or both of these condition (Fig S1 and S2). There is no justification, therefore, for removing these sectors (shaded dark grey and black in Fig S2) but it is possible that, in addition to the drawdown of ice we have estimated for the extant ice caps and EAIS margins affected by the collapse that ice streams along the Peninsula and in East Antarctic that feed the Filchner and Ross Ice Shelves, would respond to changes in the force balance due to ice shelf removal. Using the most recent estimates of mass flux for these ice streams (S4) we have estimated a possible additional dynamic contribution by assuming a doubling in grounding line velocity (a value taken based on recent observations from the largest outlet glacier in Greenland (S23)). The present-day grounding line flux is 231 Gt a^{-1} and a doubling in velocity would result in an additional 0.64 mm a^{-1} to eustatic SLR or 6.4 cm over a century. We believe, therefore, that any non-MISI response will be relatively small compared to the MISI components. We have tabulated (Table S1) the various sea level equivalent components of our calculation using the ROIs shown by the masks in Fig.s S1-S3.

4. Sea-level calculations

Our calculations of sea-level change result from the solution of the sea-level equation, as first discussed by Farrell and Clark (S24). The melting of an ice mass directly affects the Earth's gravity field, leading to a non-uniform sea-level redistribution even in the limit case of a rigid Earth. In addition, a non-rigid Earth will deform in response to the modified gravity field, instantaneously (elastic response) and on longer time-scales (relaxation). Relaxation occurs because most of the Earth mantle is capable of flowing in presence of a stress gradient.

We solve the sea level equation for a self-gravitating, spherically layered, incompressible, viscoelastic Earth with Maxwell rheology and PREM-averaged elastic and density structure, by means of a pseudo-spectral algorithm (S25) with time-varying ocean function (i.e. accounting for the fact that changes in sea-level lead to modification of the shore-lines). In addition, we analytically account for the effect of changes in the Earth's rotation axis due to mass redistribution, as described by Milne and Mitrovica (S26). Computations are performed in the spherical harmonic domain, with summation over degrees 1 to 256. The initial ice-load, represented by a uniform layer centred over the ROI with a thickness of about 1400 m, is linearly built from 120 kyr to 20 kyr before present, after that it remains

unchanged until present, and finally it linearly melts in 500 years (fast scenario) or 1700 years (slow scenario). During the melting phase, we maintain a realistic proportion between area and volume of the ice load. Since we limit our study to the effect of WAIS collapse from its current state, our results represent a contribution to global sea level variations additional to the effects of the last deglaciation and of tectonic processes.

We have benchmarked our predictions of global sea level variations for the case of a uniform melt over Greenland against the results by Mitrovica et al. (S27), obtaining an almost identical result. Our results, computed without accounting for rotational effects, are also in general agreement with Clark and Lingle (S28), the main difference being that the high-resolution of our computations (about 0.7 degrees) allows a better description of the effect of the continents. The result is a sea level pattern that is generally flatter over the oceans and with larger gradients along the coastlines. Accounting for time-varying coastlines, when the total eustatic contribution is a few meters, has a limited effect on the final solution (about 3% reduction in eustatic sea-level).

5. Effect of viscoelastic relaxation on glacial isostatic adjustment.

While the initial water redistribution due to the elastic response of the Earth is controlled by changes in the ice load (magnitude and location), the subsequent relaxation process is largely affected by the thickness of the top elastic layer (representing the lithosphere and assumed to be 100 km in this study) and by mantle viscosity. Estimates of upper mantle viscosity generally range 10^{20}-10^{21} Pa s, corresponding to a characteristic relaxation (Maxwell) time of 100-1000 years, while lower mantle viscosity ranges 10^{21}-10^{23} Pa s, with relaxation times of 1-100 kyr.

In Fig. S7 we show global sea-level at 10,000 years after present, for an Earth model with an upper mantle viscosity of $5x10^{20}$ Pa s and a lower mantle viscosity of 10^{22} Pa s, in the case of complete WAIS melt within 500 years. With respect to the elastic response shown if Fig. 2, in the Northern Hemisphere we do not have large regional variations, the relative sea level being close to eustatic at most locations. However, ongoing relaxation is still clearly visible in the peripheral bulge around the WAIS, where the large positive relative sea level is mainly due subsidence of the sea bottom. Finally, the effect of Earth rotation is also drastically reduced, now barely visible in the small area with values above 1.1 at the west coast of North America.

The second important consequence of glacial isostatic adjustment is that relative sea-level changes within the newly inundated ROI can largely affect eustatic sea-level. This process, commonly referred to as 'near-field water dumping', has been discussed by Milne et al. (S29), who have also proposed a way to incorporate it in the sea-level equation. However, since in our case water dumping is limited to a restricted and known basin (the ROI) and to a moderate variation in eustatic sea-level, we compute it 'a posteriori', by simply integrating relative sea-level changes within the ROI at each time step. In this way, the only approximation we perform is that we do not account for variations in the ocean bottom pressure within the ROI, which has a very limited impact on the final solution as the maximum variation is less than 250 m and confined to a relatively narrow region.

In Fig. S8 we show a plot of near-field relative sea-level at 10,000 years after present, for the same Earth model as above. Note that the scale is in meters. The large sea level drop under the former ice load is mainly due to uplift of the solid Earth surface and means that a large volume of water (about $2x10^5$ km^3 when integrated over the ROI) has been driven out of the ROI and distributed over the oceans (resulting in about 54 cm of eustatic sea-level rise). Sea-level changes over regions that were already inundated before the beginning of WAIS melt are already self-consistently included in our computations when accounting for shore-line migration.

The additional 54 cm have been included in the centimetre scale of Fig. S7, leading to a total 3.80 m eustatic sea-level. The fact that the eustatic value is only 14% higher than the elastic contribution shown in Fig. 2 means that, when comparing Fig. 2 and Fig. S7, the most obvious difference is a slight sea level reduction in the Northern Hemisphere in the latter.

However, even if the normalized sea-level changes of Fig. S7 are still valid in the case of a partial WAIS collapse (as for Fig. 2), the same is not true for the centimetre scale, neither for the results of Fig. S8 or S9, which have been computed in a scenario where complete collapse actually occurs. This means that, if we only removed a thin ice layer from the ROI, the Northern Hemisphere would experience a moderate sea level drop as a result of isostatic adjustment (as in (S28)).

6. Effect of deglaciation rate and mantle viscosity.

In this section we study the effect of the two proposed melting scenarios and of two different mantle viscosity models on the additional eustatic contribution due to glacial isostatic adjustment within the ROI. In Fig. S9 we show a plot of eustatic sea level as a function of time for the ROI: all curves share the same general trend, consistent with uplift of the Earth's surface as a consequence of the reduced ice load. The global elastic and viscous deformation of the oceans due to loading reduces the values plotted in Fig S9 by 6 cm at 10000 years. The difference between the fast (complete melt in 500 years) and slow (complete melt in 1700 years) scenarios is largest in the first 1700 years: partial WAIS melt does not only mean that both the elastic response and the effect of relaxation are smaller, but also that the ROI is only partially inundated, limiting the amount of water that can be poured into the oceans. After complete melt both scenarios show a very similar relaxation rate, consistently with the fact that the initial ice load is the same. As far as the impact of upper mantle viscosity is concerned, a lower viscosity implies faster relaxation rates, which is clearly visible in the first few thousands of years: for longer times the lines remain almost parallel, because relaxation becomes mainly controlled by the viscosity of the lower mantle, which is in both cases the same.
We have also tested a model where the whole mantle has a uniform viscosity of 10^{21} Pa s, but results are very close to the red lines, since the effect of a faster relaxing lower mantle is mostly compensated by a slower upper mantle.

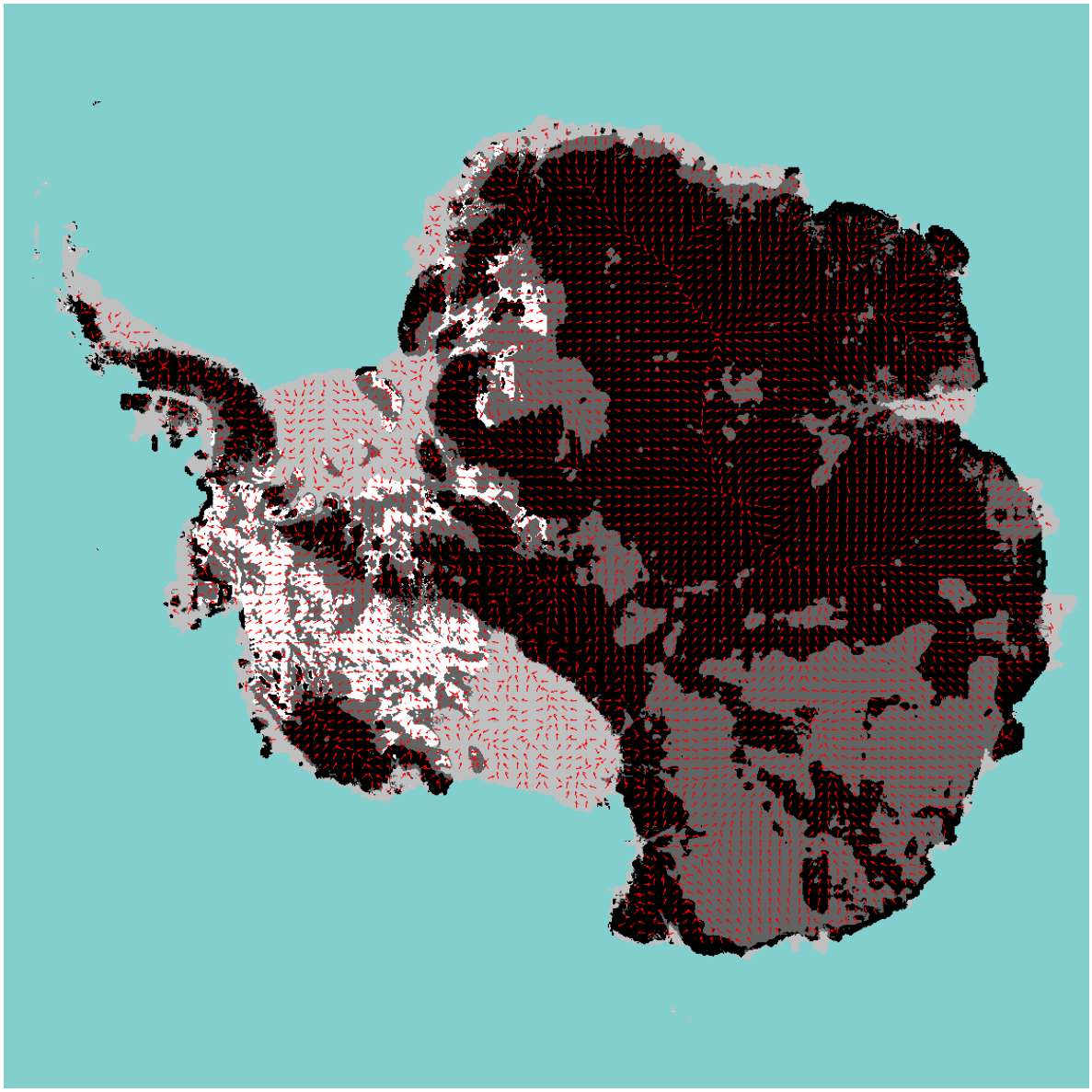

Fig S1. A plot of grid cells that satisfy the Marine Ice Sheet Instability condition for West Antarctica as defined in section 2 (shown in white), areas of bed below sea level (dark grey) and bed areas above sea level (black). The red arrows are surface slope vectors indicating the upstream ice motion direction derived from the smoothed digital elevation model. Light grey areas show the extent of the present-day ice shelves.

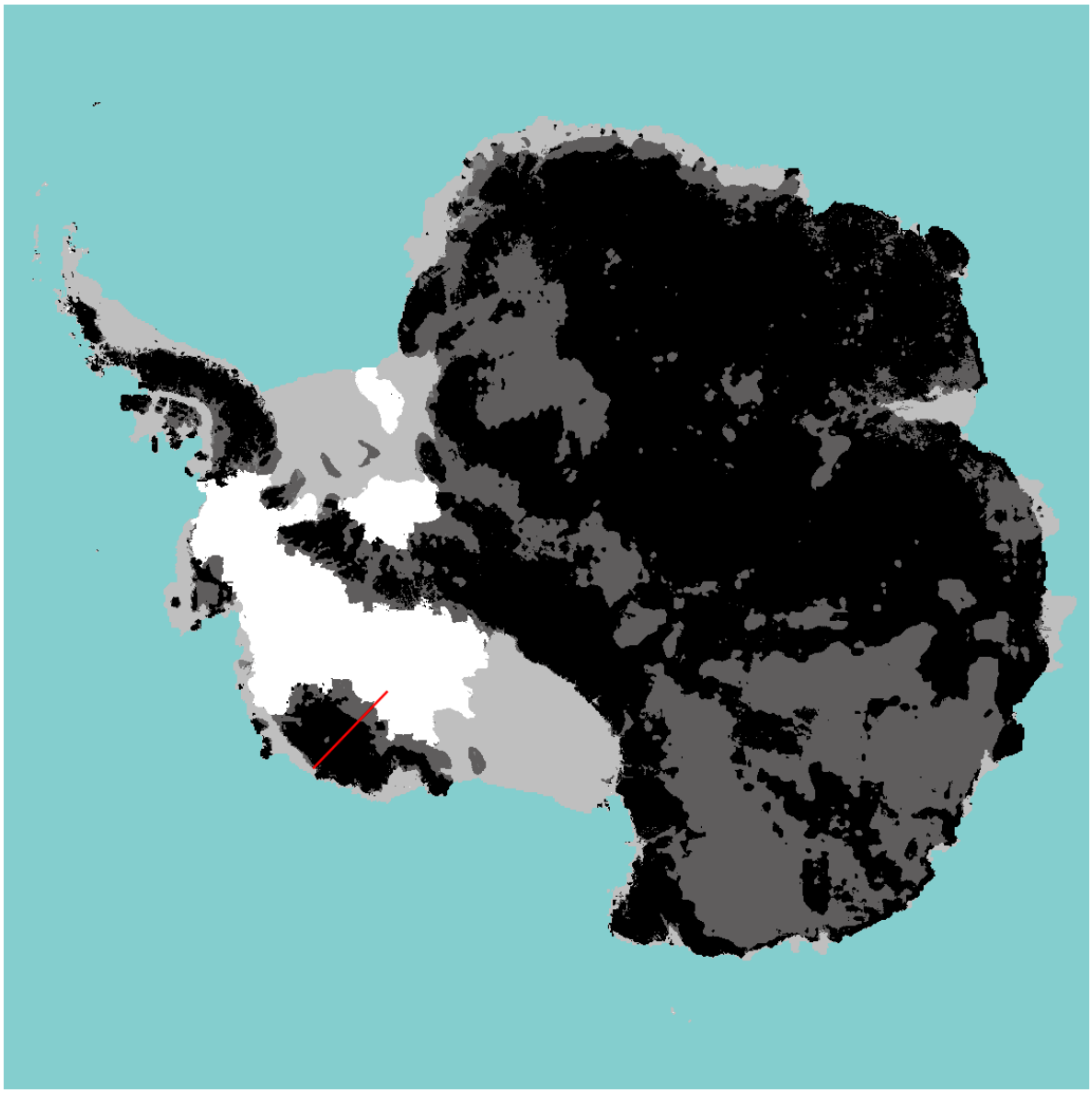

Fig S2. The mask used to estimate those areas that are lost from a collapse of the WAIS (shown in white), areas that remain, but which are below sea level (dark grey) and areas above sea level (black). The solid red line indicates the locations of the surface and bed profile plotted in Fig. S5. Light grey areas show the extent of the present-day ice shelves.

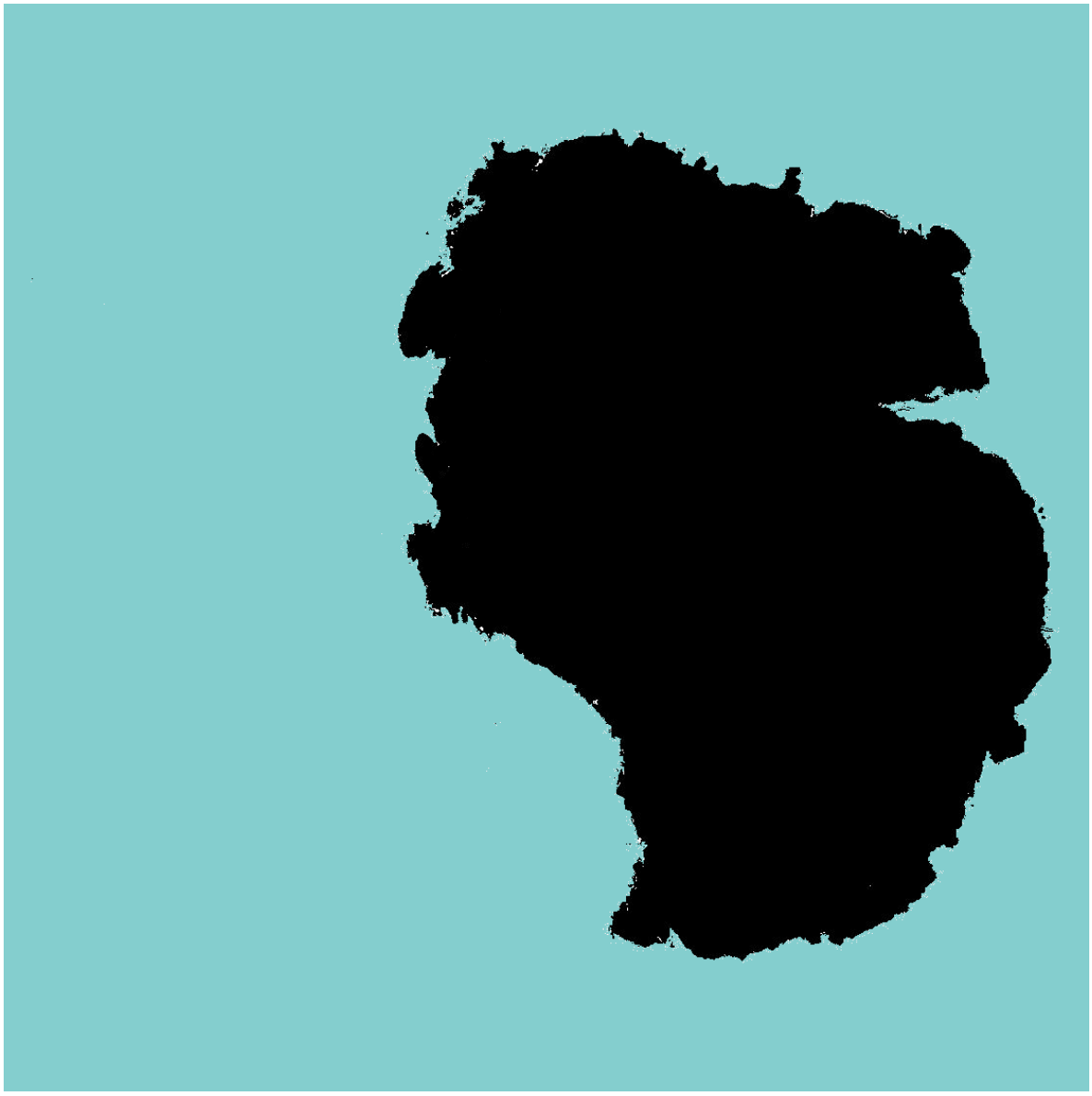

Fig S3. The mask used to estimate the sea level equivalent volume for the entire WAIS and Antarctic Peninsula, making no assumptions about bed elevation or slope.

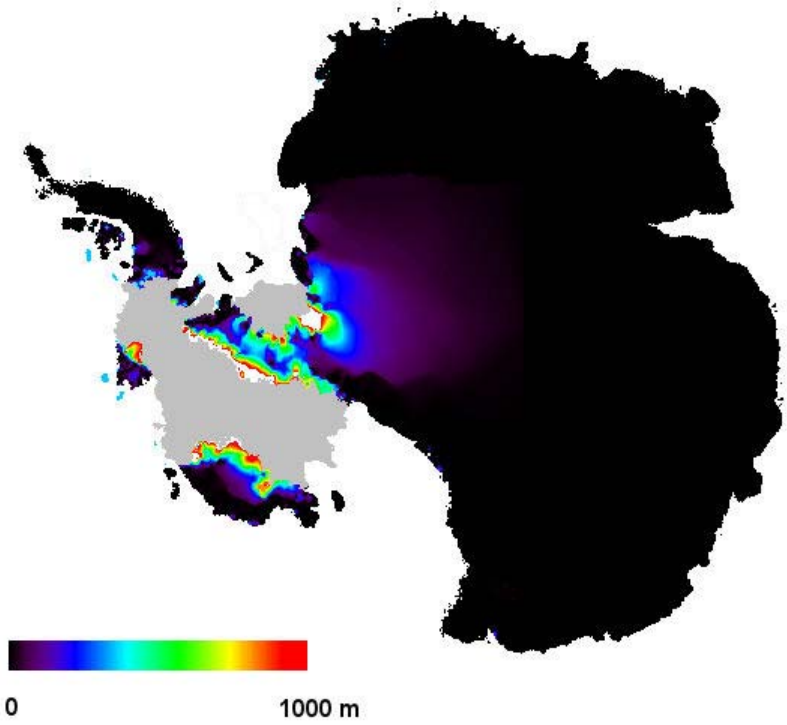

Fig S4. The difference in ice thickness between the present-day numerical model simulation and one where the areas shaded grey were forced to be non-ice sheet points. Large differences, exceeding 1000 m, are evident for the EMIC and MBLIC but also for the newly created margins of Recovery Glacier and Foundation ice stream. At equilibrium, the impact for this part of the EAIS extends as far as the South Pole.

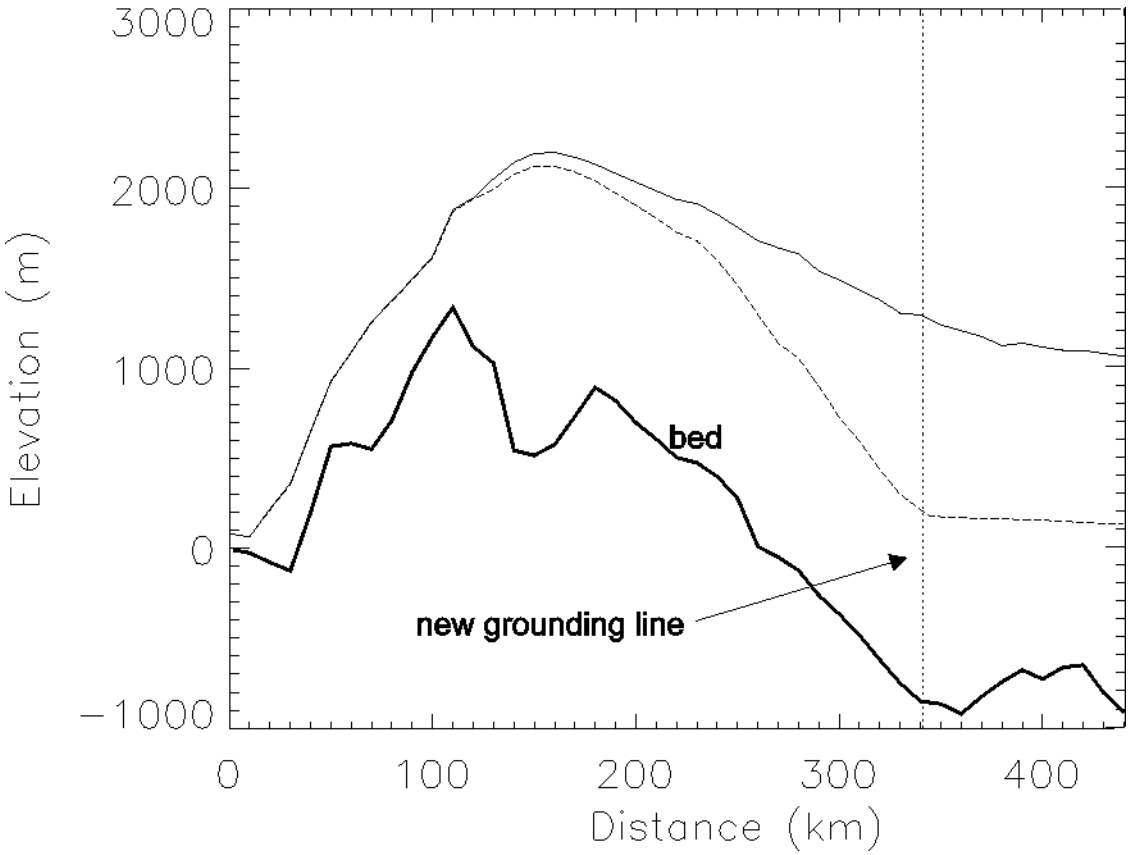

Fig S5. North-south profile across the width of Marie Byrd Land Ice Cap (MBLIC) showing the original surface and bed topography in solid and the "relaxed" surface topography as a dashed line. The new grounding line is located at ~340 km. At this point, the boundary condition for the surface elevation is hydrostatic equilibrium. The location of the profile is shown in Fig. S2 by the solid red line.

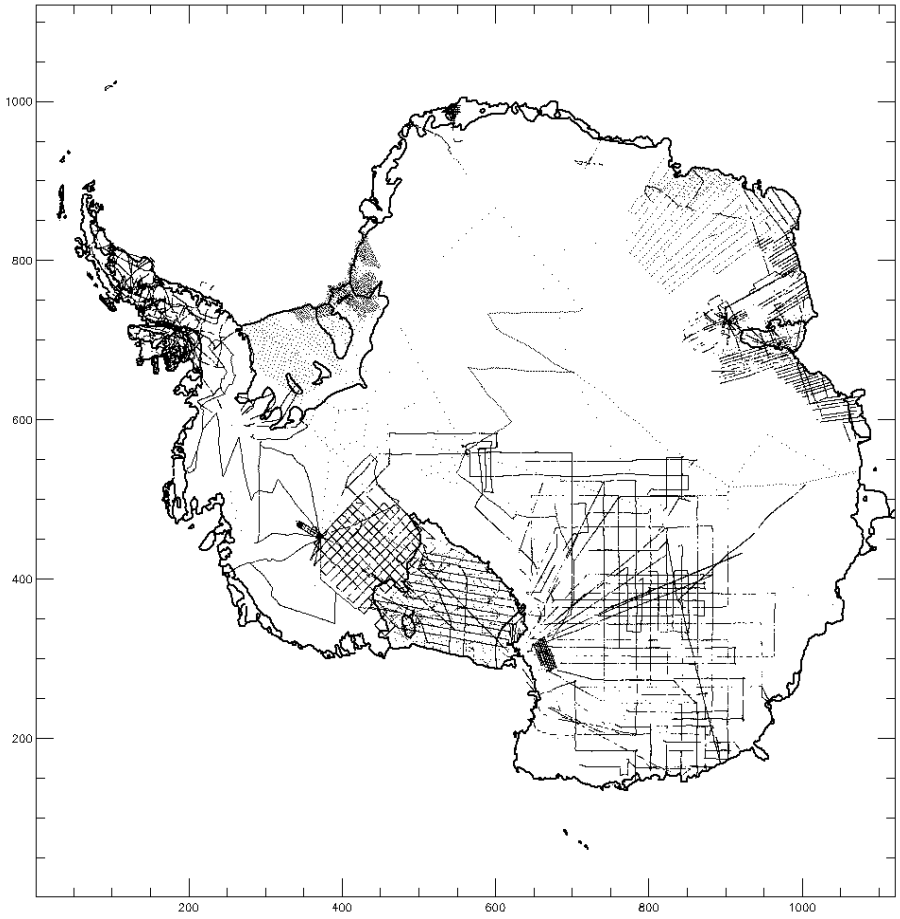

Fig S6. Ice thickness data coverage over Antarctica up to 1978. Only the Siple Coast region of the WAIS has adequate coverage to produce reliable bed and surface topography.

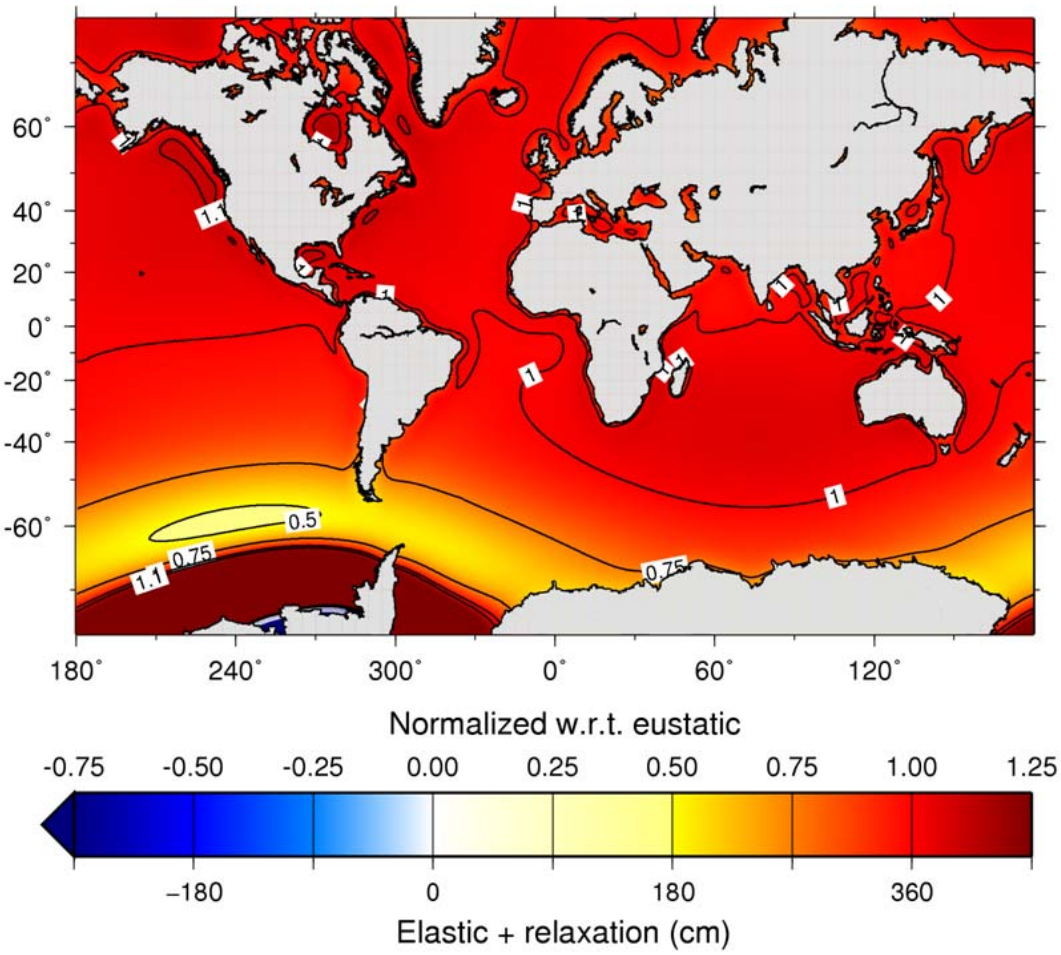

Fig. S7. Sea-level changes at 10,000 years after present, in the fast melt scenario, for an Earth model with a viscosity of 5×10^{20} Pa s in the upper mantle and 10^{22} Pa s in the lower mantle.

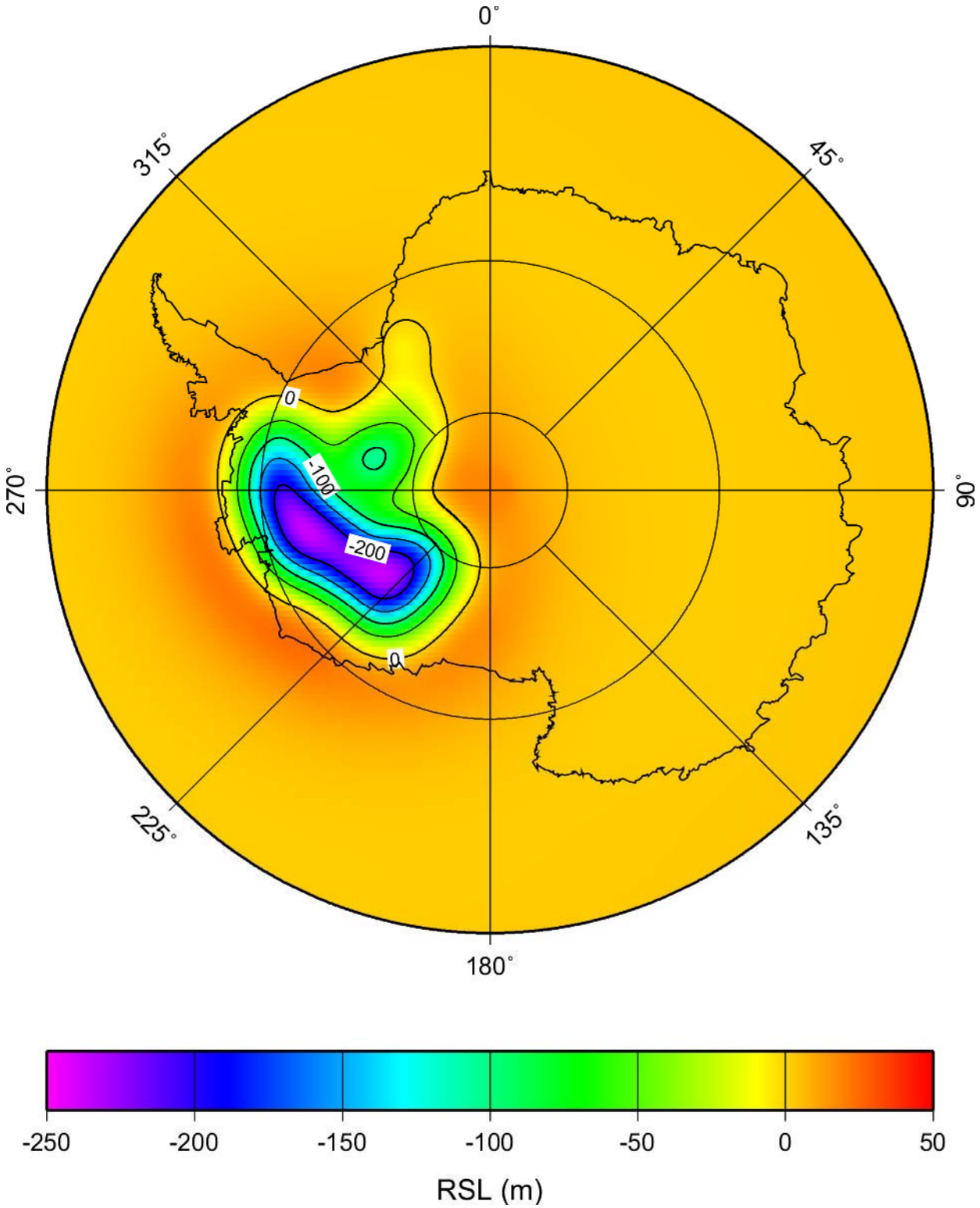

Fig. S8. Near-field relative sea-level changes at 10,000 years after present, for the same situation as in Fig. S6.

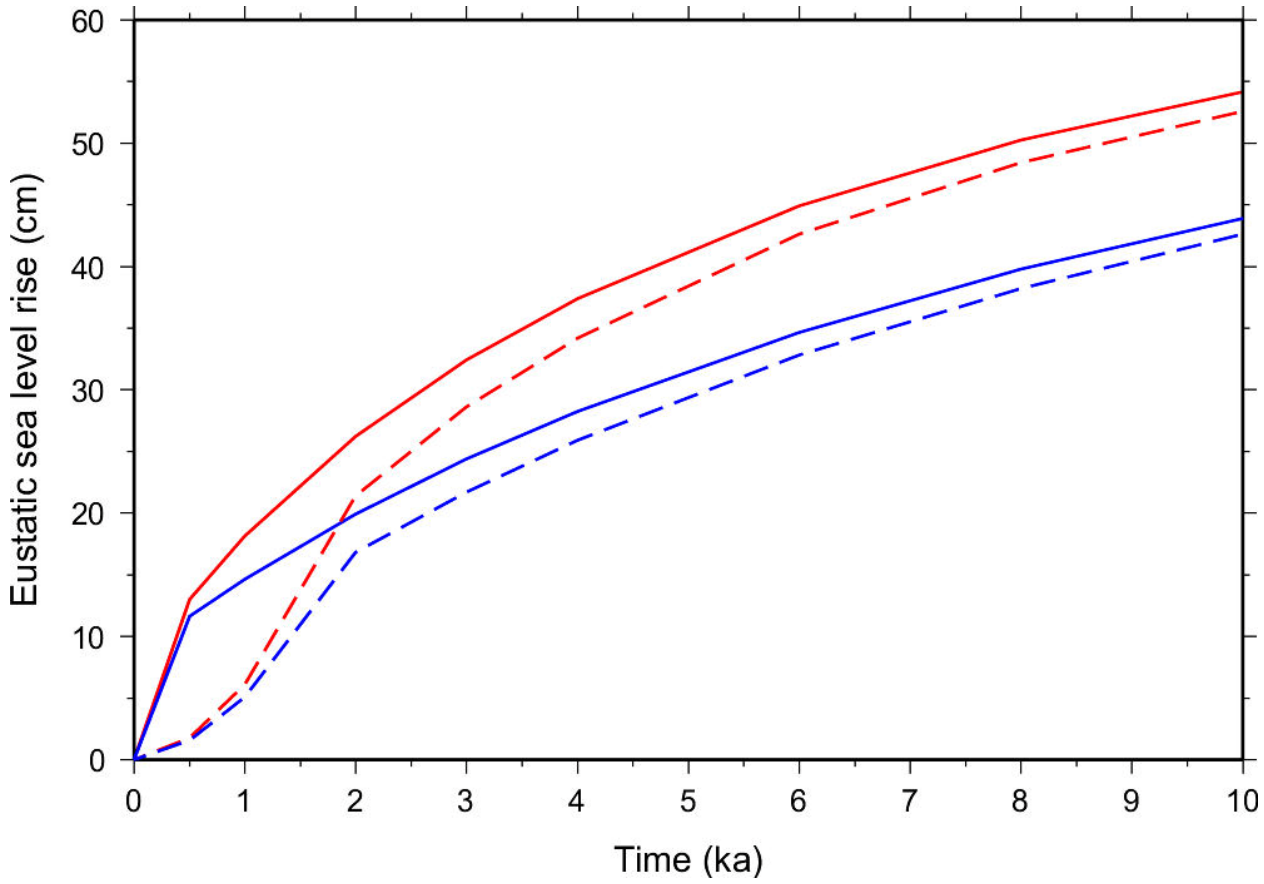

Fig. S9. Eustatic sea-level rise as a function of time due to viscoelastic relaxation within the ROI, for the fast (solid lines) and slow (dashed lines) melt scenarios, for an Earth model with soft (red lines) and hard (blue lines) upper mantle (viscosity of 5×10^{20} Pa s and 10^{21} Pa s respectively) and a lower mantle viscosity of 10^{22} Pa s. This plot does not include the response of the global oceans to increased loading, which is -6 cm at 10000 years.

Table S1. Estimates of the sea level equivalent contributions from various sources and scenarios.

Scenario	See level equivalent volume (cm of sea level)
1. Strictly satisfying MISI conditions (Fig S1)	126
2. Satisfying MISI conditions as described in manuscript (Fig S2)	246 (+ 74 from drawdown)
3. Removal of all ice in West Antarctica including Peninsula (Fig S3)	480
4. Contribution of drawdown of extant ice caps during collapse	54
5. Contribution of drawdown of EAIS during collapse	20
6. Contribution of EAIS and AP dynamic response to loss of ice shelves	0.64 mm a^{-1} => 6.4 cm over 100 years
7. Effect of ocean freshening (S30)	3% => additional ~ 8 cm, assuming no change in ocean temperature (S30)
8. Extant ice grounded ASL before drawdown; After drawdown	151 134
9. Extant ice grounded BSL before drawdown; After drawdown	80 44
10. Elastic response of lithosphere	6

1. Volume of ice defined by the area shown in Fig S1 where the MISI conditions are satisfied excluding any assumptions about the impact on adjacent ice areas. No relaxation correction has been included in this value (see 4)
2. Volume of ice defined by the area shown in Fig S2 where the MISI conditions are satisfied and including the assumption that isolated adjacent ice areas grounded BSL will be affected as described in the main report.
3. Complete removal of the whole of WAIS as indicated in by the area remaining/lost in Fig S3. No relaxation correction has been included (see 4). The effect of the firn correction reduces the estimate by 11 cm for this scenario.
4. The impact of drawdown of extant ice in the WAIS using the approach described in section 2 and illustrated in Fig S4. This value was calculated for scenario 2 (Fig S2).
5. The impact of drawdown in the EAIS using the approach described in section 2 and illustrated in Fig S4.
6. Estimate of additional contribution from EAIS glaciers flowing into the Filchner and Ross ice shelves, as a response to their removal. Their response is unlikely to be constant through time and our estimate is based on observations of the response of Jakobshavn Isbrae to loss of its floating tongue (S23). The speed-up of this glacier has been maintained for ~a decade.

7. The salinity of the ocean is affected by the introduction of large volumes of freshwater. Assuming no change in temperature, the impact of this is 3% of the contribution (S30). For a contribution of 260 cm (scenario 2) this results in an additional 8 cm of SLR. However, as suggested by Jenkins and Holland (2007), most of the energy required to melt this volume of ice will come from the ocean resulting in a reduction in mean oceanic temperature. 8 cm is, thus, a maximum upper limit.
8. This is the volume of ice that is grounded above sea level that is assumed to survive, before and after drawdown. No glaciologically plausible scenarios include this ice.
9. This is the volume of marine-based ice (lying on bedrock above -1000 m), which, according to our calculations, does not satisfy the condition of possessing a negative bed-slope, after relaxation to a post collapse profile.
10. The elastic response of the lithosphere to the change in loading is rapid (Fig S9) and is, therefore, included in our estimate of the eustatic SLR as a result of collapse. In the ROI the value is 9 cm (Fig S9) but the global value is reduced to 6 cm by the elastic response of the global oceans to increased loading.

References

S1. J. H. Mercer, *Nature* **271**, 321 (1978).
S2. H. De Angelis, P. Skvarca, *Science* **299**, 1560 (2003).
S3. E. Rignot *et al.*, *Geophys. Res. Lett.* **31**, art. No. L18401 (2004).
S4. E. Rignot *et al.*, *Nature Geosci* **1**, 106 (2008).
S5. E. J. Rignot, *Science* **281**, 549 (J1998).
S6. R. H. Thomas, T. J. O. Sanderson, K. E. Rose, *Nature* **277**, 355 (1979).
S7. R. B. Alley, P. U. Clark, P. Huybrechts, I. Joughin, *Science* **310**, 456 (2005).
S8. D. Vaughan, *Climatic Change* **91**, 65 (2008).
S9. F. Pattyn, *J. Geophys. Res.***108**, doi. 10.1029/2002JB002329 (2003).
S10. F. Pattyn, A. Huyghe, S. De Brabander, B. De Smedt, *J. Geophys. Res* **111**, F02004 (2006).
S11. C. Schoof, *J. Geophys. Res.* **112**, F03S28 (2007).
S12. J. H. Mercer. (IAHS, 1968), vol. 79, pp. 217-225.
S13. A. Shepherd, D. Wingham, *Science* **315**, 1529 (Mar, 2007).
S14. J. L. Bamber *et al.*, *Geology* **34**, 33 (Jan, 2006).
S15. I. Joughin *et al.*, *Phil. Trans. R. Soc. A* **364**, 1795 (2006).
S16. A. M. Le Brocq, A. Hubbard, M. J. Bentley, J. L. Bamber, *Geophys. Res. Lett.*, doi:10.1029/2008GL034728 (2008).
S17. B. Kamb, K. A. Echelmeyer, *J. Glaciol.* **32**, 267 (1986).
S18. I. Rutt, M. Hagdorn, N. R. J. Hulton, A. J. Payne, *J. Geophys. Res.*, doi:10.1029/2008JF001015 (2009).
S19. S. S. Vialov, *International Association of Hydrology, Scientific Publication* **47**, 266 (1958).
S20. R. H. Thomas, *J. Glaciol.* **24**, 167 (1979).
S21. M. M. Helsen *et al.*, *Science*, 1153894 (2008).
S22. M. B. Lythe, D. G. Vaughan, *J. Geophys. Res.* **106**, 11335 (2001).
S23. I. Joughin, W. Abdalati, M. Fahnestock, *Nature* **432**, 608 (2004).

S24. W. E. Farrell, J. A. Clark, *Geophys. J. R. astr. Soc.* **46**, 647 (1976).
S25. G. Di Donato, L. L. A. Vermeersen, R. Sabadini, *Tectonophysics* **320**, 409 (2000).
S26. G. A. Milne, J. X. Mitrovica, *Geophys. J. Int.* **133**, 1 (Apr, 1998).
S27. J. X. Mitrovica, M. E. Tamisiea, J. L. Davis, G. A. Milne, *Nature* **409**, 1026 (2001).
S28. J. A. Clark, C. S. Lingle, *Nature* **269**, 206 (1977).
S29. G. A. Milne, J. X. Mitrovica, J. L. Davis, *Geophys. J. Int.* **139**, 464 (1999).
S30. A. Jenkins, D. Holland, *Geophys. Res. Lett.* **34** doi: 10.1029/2007GL030784 (2007).